Elastic scattering and fusion of ^{9}Be+^{208}Pb: Density function dependence of the double folding renormalization

R. J. Woolliscroft
School of Physics and Astronomy, University of Birmingham, Edgbaston, Birmingham B15 2TT, United Kingdom

B. R. Fulton and R. L. Cowin
Department of Physics, University of York, Heslington, York YO10 5DD, United Kingdom

M. Dasgupta, D. J. Hinde, C. R. Morton, and A. C. Berriman
Department of Nuclear Physics, Research School of Physical Sciences and Engineering, Australian National University, Canberra ACT 0200, Australia

(Received 18 December 2001; revised manuscript received 9 January 2004; published 26 April 2004)

Elastic scattering angular distributions of the weakly bound ^{9}Be projectile from ^{208}Pb have been measured for 11 beam energies ranging from 38 to 75 MeV. Analysis was carried out with the optical model, employing a double folded microscopic real potential with four different ^{9}Be density functions. The surface strengths of the interaction potentials were consistent and all exhibited a threshold anomaly. However, the renormalization factor required to obtain an optimum fit to the data varied significantly depending upon which ^{9}Be density function was used, cautioning that conclusions about the effect of breakup should not be based solely upon the value of this factor. Fusion cross sections predicted from these potentials were extracted using a barrier penetration model. Comparison with recently published experimental data suggests that the flux removed from complete fusion by breakup is balanced by the flux redirected into the partial fusion channel.

DOI: 10.1103/PhysRevC.69.044612 PACS number(s): 25.70.Bc, 25.70.Jj

I. INTRODUCTION

Interest in the effect of breakup on the reactions of weakly bound nuclei has been revived recently due to the increasing use of radioactive beams. These beams are expected to exhibit their weak binding by strong coupling to the breakup channel, which will modify the flux to the other channels. It will be important to understand the nature of such couplings using presently available stable beams before studying radioactive isotopes, whose more exotic structures may complicate the couplings further.

In particular, we already know from studies of reactions with the most weakly bound stable nuclei, ^{6}Li, ^{7}Li, and ^{9}Be, that a number of problems occur. The normally successful double folding model fails for these nuclei [1], ^{6}Li does not display the usual threshold anomaly at energies near the Coulomb barrier [2,3], and, contrary to expectations, the ^{9}Be fusion cross section at low energies does not appear to differ from that of the much more diffuse ^{11}Be nucleus [4].

A. Failure of the double folding model for weakly bound nuclei

The conventional approach to describe the elastic scattering between two nuclei is in terms of the optical model, using a complex potential. Often the potential is parametrized in terms of some standard form, for example, a Woods-Saxon shape, with the values of the parameters adjusted to give the best fit to the elastic scattering angular distribution. An alternative approach is to use the double folding model, in which the real part of the potential is calculated by summing the individual interactions between all the nucleons in the two nuclei. As well as putting the description on a more microscopic basis, this approach is also more appropriate when examining the variation of elastic scattering over a range of bombarding energies, since the same potential should be appropriate for all energies.

The calculation of the double folding model potential involves an integration over the nucleon density distributions in the two nuclei using an effective nucleon-nucleon interaction $V(r_1-r_2)$:

$$V(r) = \int \rho(r_1) V(r_1 - r_2) \rho(r_2) dr_1 dr_2. \quad (1)$$

The nuclear density distributions may be taken from experimental measurements (for example, electron scattering) or from theoretical calculations (for example, shell model or Hartree-Fock wave functions). An effective interaction is used, rather than the bare nucleon–experimental detail nucleon interaction, since the nuclei are embedded in nuclear matter and so certain scatterings will be blocked. A number of prescriptions exist for obtaining the effective interaction strating from the nucleon-nucleon interaction, one of the most popular being the M3Y interaction [5], including recent extensions of this such as the BDM3Y1 interaction which incorporates density dependent effects [6]. In a seminal work on the double folding model, Satchler and Love [1] showed that, with a few specific exceptions, the potentials could describe elastic scattering for a wide range of heavy ion collisions, over a broad energy range.

The exceptions identified by Satchler and Love were systems involving the nuclei ^{6}Li, ^{7}Li, and ^{9}Be the most weakly bound of the stable isotopes. In these cases, the double folding potential cannot reproduce the elastic scattering data unless the potential is considerably weakened, typically by a

 ©2004 The American Physical Society

factor of ~0.6. This finding has been confirmed in a large number of measurements on many different target nuclei [2,7,8]. It was suggested [1] that this failure arises because breakup effects are important for these projectiles—they have the lowest breakup threshold energy of the stable nuclei. This conjecture has been confirmed theoretically, in particular, by the coupled discretized continuum channel (CDCC) calculations of Sakuragi *et al.* [7,8] for ^{6}Li. In these calculations the coupling to breakup is included and the elastic scattering is then reproduced without the need to renormalize the potential. However, as yet these have been no experimental measurements of the breakup yield to check the calculations.

One problem which Satchler and Love experienced in carrying out their double folding calculations for ^{9}Be was the lack of a suitable density for this nucleus, leading to some uncertainty in the calculated potential and hence in the absolute value of the renormalization required to fit the elastic scattering. We now have available more realistic ^{9}Be wave functions from which the densities can be derived; shell model [1], cluster model [9], and antisymmetrized molecular dynamics calculations [10] all having been reported recently. In view of this it is important to see whether the normalization is different for these (hopefully) more realistic densities.

B. The threshold anomaly in weakly bound systems

Keeley *et al.* [2] have recently investigated the elastic scattering of ^{6,7}Li + ^{208}Pb at a range of energies from below the barrier to well above the Coulomb barrier. The aim of that investigation was to see whether the renormalization persisted to lower energies and, in particular, to see whether these systems display a "threshold anomaly." This refers to the rapid increase in the strength of the real part of the optical potential as the scattering energy decreases towards the barrier energy. First observed in the scattering of ^{16}O + ^{208}Pb [11], it has subsequently been observed in many other systems [12,13] and is considered a normal feature of heavy ion scattering. The rise of the real potential is understood in terms of a dispersion relation between the real and imaginary parts of the potential and is due to the rapid decrease in the strength of the imaginary potential as reaction channels become energetically closed as the barrier is approached.

The measurements of Keeley *et al.* showed that for the ^{6}Li projectile the depth of the real potential remained unchanged (at a renormalization of ~0.6 for the double folding potential) for energies down to the barrier. By contrast, for the ^{7}Li projectile a threshold anomaly is observed, with the depth of the real potential increasing as the barrier energy is approached, where a renormalization factor of $N=1.5$ is observed. Keeley *et al.* showed in a later paper [14], using a CDCC method, that it was the lower breakup threshold of ^{6}Li that gave rise to a dominant breakup channel. As this channel did not close at the Coulomb barrier there was little change to the imaginary polarization potential, hence no observed threshold anomaly. This conclusion has been supported in a separate study of ^{6,7}Li using a CDCC method [3].

Based on a comparison of the breakup threshold of ^{9}Be compared to that of ^{6}Li and ^{7}Li, Keeley [14] has suggested that ^{9}Be may not exhibit a threshold anomaly as its dissociation threshold is closer to that of ^{6}Li. Signorini *et al.* [15] measured elastic scattering for the ^{9}Be + ^{209}Bi system at five energies around the barrier energy and report an unusual behavior in the optical potential. Although the real potential strength appears to show a peak at the barrier, the imaginary potential strength is steeply rising in this region—at odds with other systems and inconsistent with a dispersion relationship between real and imaginary parts of the complex potential. However, Signorini *et al.* caution that no conclusions should be drawn as there are not enough data points. The present study aims to provide a more comprehensive data set extending to lower and higher energies.

C. Suppression or enhancement of fusion for weakly bound nuclei

The question of whether coupling to breakup channels will enhance or hinder fusion is a topic of current interest. A particular interest in ^{9}Be fusion arises from recent studies on ^{9}Be + ^{208}Pb fusion [16], and the neighboring ^{9}Be + ^{209}Bi system [4,17]. The former measurement showed that there is a discrepancy in the complete fusion yield, which is only 70% of that expected. However, this missing flux seems to appear in the partial fusion channels (α + ^{208}Pb) and the authors suggest [14] that this is explained by the breakup of the projectile, followed by the capture (fusion) of one of the fragments. The presence of a strong partial fusion yield persists down to the lowest energies, below the Coulomb barrier. It is of interest to investigate whether the potential obtained from the anslysis of the elastic scattering data can explain the measured fusion plus partial fusion yields, given that the breakup should affect both the elastic and the fusion channels.

Knowledge of the influence of breakup on fusion is also needed to understand the relative fusion yields of ^{9}Be and ^{11}Be. ^{11}Be is a Borromean nucleus, consisting of a ^{9}Be core with two valence neutrons. This more diffuse nuclear density distribution would be expected to enhance its fusion cross section. Although this has been observed to be the case above the Coulomb barrier, below it the cross sections are similar to ^{9}Be [4], which is not well understood.

II. EXPERIMENTAL DETAILS

Experience has shown that it is only possible to extract unambiguous information on the potential if high quality ($\leqslant$2% uncertainty) elastic scattering data are obtained over a very wide angular range at each bombarding energy. This requires considerable attention to detail in the experiment.

The experiment was performed, using the 14UD Tandem Van de Graaff accelerator at the Australian National University, Canberra. The ^{9}Be beam was operated at energies of 38.0–52.0 MeV in steps of 2.0 MeV and 60.0, 68.0, and 75.0 MeV. The beam was tightly collimated to produce a beam spot of 1×2 mm^2 at the target, which comprised 180 μg cm^{-2} $^{208}PbCl_2$ on a 15 μg cm^{-2} natural carbon backing.

To detect the scattered particles, three silicon position sensitive detector (PSD) $\Delta E-E$ telescopes were employed. The

passing ΔE detectors were 69 μm thick, and the stopping E detectors were 500 μm thick. Each detector had a sensitive area of 10×50 mm^2, and was position sensitive along the longer dimension. The telescopes were mounted on separate horizontally rotatable arms. For angular definition, masks were placed over the telescopes. These had ten vertical slots cut into them to create ten position bins $\approx 1°$ wide.

In the offine analysis, a $\Delta E-E$ spectrum was created for each telescope, and a two-dimensional window used to select ^{9}Be particles, which were clearly identifiable at all angles and beam energies. This ensured that no contribution from positive Q-value transfer channels was included. Gates were then applied to the peaks in the position spectra which corresponded to each of the separate slots in the mask, to enable separate energy spectra to be generated for each angle. Finally, the counts in the elastic peaks were summed to determine the elastic yield.

Other particle types were visible in the $\Delta E-E$ spectra. Analysis of these data is presented in another paper [18].

To provide an absolute normalization for the scattering yield, two monitor detectors were used. These were silicon surface barrier detectors, positioned at $\pm 15°$ to the beam and in the plane of the PSD telescopes. For determination of the absolute cross sections, the ratio of the solid angles of the monitors to each slit on each telescope had to be determined. This was achieved by performing a calibration run at a beam energy of 36.0 MeV. The telescopes were placed at the smallest angles possible ($\pm 25°$), where at this beam energy it is safe to assume that the elastic scattering cross section is Rutherford. The ratio of the solid angles of the monitors and each position bin in each detector was then determined from the ratio of the number of observed elastic events in each.

The dead time associated with the electronics and data acquisition system was determined for each run. This was achieved by injecting electronic pulses into the preamplifiers at a rate proportional to the beam intensity. The ratio of pulser signals presented to those recorded was used to correct the elastic counts. This correction was never more than a few percent.

The elastic scattering data, presented as the ratio of the measured differential cross sections to those for Rutherford scattering, are shown in Fig. 1, identified by their beam energy [28].

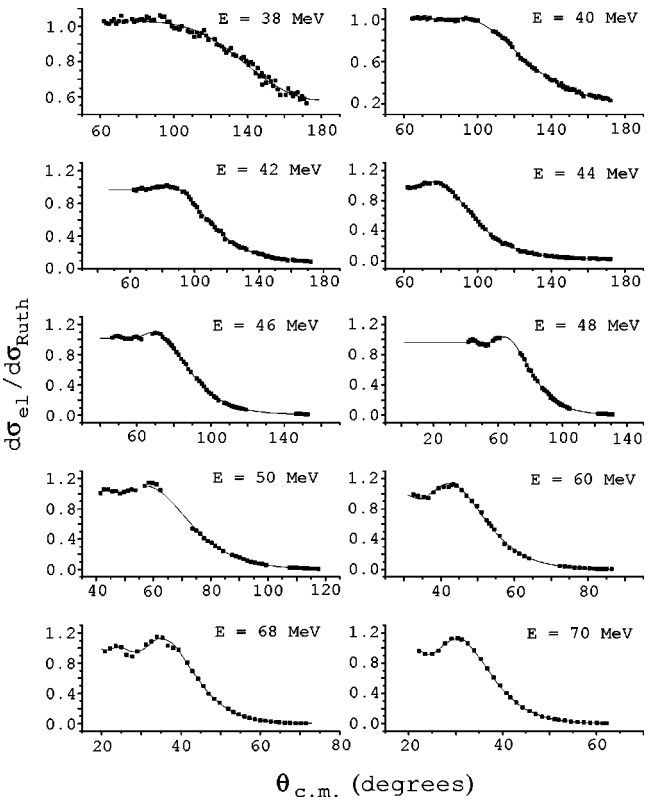

FIG. 1. The measured angular distributions with optical model fits.

III. OPTICAL MODEL ANALYSES

A. The fitting methodology

The results were fitted using the code HIOPTIM94 [19], using a microscopic potential for the real part of the interaction potential, and a Woods-Saxon form for the imaginary part. The microscopic double folded potential was calculated using the code DFPOT [19] in which the ^{208}Pb density was derived from a Hartree-Fock calculation. The calculation was repeated using four density functions for the ^{9}Be nucleus, each giving a different microscopic potential. The effective interaction used was the Reid form of the M3Y interaction [20].

One density function used a harmonic oscillator shape, parametrized to fit the ^{9}Be radius measured by electron scattering [21]. The others used theoretical wave functions; shell model [22], a full antisymmetrized cluster model [9], and an antisymmetrized molecular dynamics (AMD) model [10].

The fitting procedure was repeated using each double folding potential. In each procedure, searches were initially conducted with all parameters of the potentials free. These parameters were the renormalization of the double folding potential N_R and the three parameters which described the Woods-Saxon imaginary potential (the depth W, the radius R_W, and the diffuseness a_W). The absolute normalization, NORM, of the data was fixed in each search, and incrementally altered in repeated searches to find the optimum normalization. This allowed a check on the experimental normalization of the data, although this had little effect on the optimum potential parameters. The deviation of NORM from 1.0 reflects the experimental uncertainties.

For the main analysis, once the normalization had been fixed, the highest energy data set was analyzed first, as it displays the most pronounced Coulomb-nuclear interference in the angular distribution (see Fig. 1). The parameters from this data set were used as the initial search parameters of the next energy down and successively to the lowest energy. This method was employed because the quality of the fit to the data within these peaks is particularly sensitive to the parameters used, thus these peaks help constrain the parameters required to achieve an optimum fit. To avoid the ambiguities usually associated with analyses of this kind, the average radius parameter of the imaginary potential from the initial searches was used as a fixed parameter for all data sets in a repeated search. This had little effect in the quality of fit to

TABLE I. Best fit parameters for optical model fits to ^{9}Be $+^{208}$Pb elastic scattering using a ^{9}Be density based upon harmonic oscillator wave functions. R_W fixed at 1.37 fm.

E_{LAB}(MeV)	N_R	W(MeV)	a_W(fm)	NORM	χ^2_N
75	0.893	6.96	0.701	0.972	7.0
68	0.872	6.60	0.713	0.988	13.3
60	1.006	8.78	0.650	0.990	14.4
52	1.401	8.08	0.668	1.051	36.7
50	1.000	11.11	0.621	1.045	18.9
48	1.085	11.74	0.530	0.965	7.4
46	1.223	12.93	0.500	1.020	5.3
44	1.439	15.91	0.434	0.971	1.7
42	1.736	27.93	0.396	0.970	4.7
40	1.286	13.77	0.509	0.999	4.5
38	1.154	2.98	0.812	1.034	6.5

the data. Typical best fits to angular distributions are shown in Fig. 1, and the optimum fit parameters are tabulated in Tables I–IV. Searches on the 52.0 MeV data set consistently yielded poor fits, with χ^2 values many times that of the other data sets. For this reason this data set was removed from the analysis.

B. Energy dependence of the potentials

The threshold anomaly is usually investigated by looking at the strength of the potential in the surface region since it is in that region that the reactions which give rise to it through the dispersion relation are concentrated (in general, a dispersion relation linking real and imaginary potentials will exist at all radii). We have chosen a value of $R=12.3$ fm to explore this aspect, since this is the region where the elastic scattering data are most sensitive to the strength of the potential. This was determined in the usual way [2] by performing repeated searches on the data with Woods-Saxon real potentials of different diffuseness and finding the point at which they all cross. Figure 2 shows the variation with beam energy of the strength of the real and imaginary potentials in the surface region ($R=12.3$ fm) derived from the analysis with each of the four radial densities. All show the same energy variation and increase from 0.7 to around 1.2 MeV as the Coulomb barrier is approached. The error bars on the points represent the change in potential which produces a change in the χ^2 value by 15%.

Inspection of Fig. 2 shows that the ^{9}Be$+^{208}$Pb system appears to show a threshold anomaly. Of the two other very weakly bound stable nuclei, ^{6}Li and ^{7}Li, ^{6}Li does not exhibit a threshold anomaly [2], and this has been attributed to its slightly lower dissociation threshold with respect to ^{7}Li [14] ($^{6}\mathrm{Li}\rightarrow\alpha+d$ at 1.47 MeV compared to $^{7}\mathrm{Li}\rightarrow\alpha+t$ at 2.47 MeV. Kelley and Rusek [12] carried out CDCC calculations which appear to support this view, since by artificially lowering the ^{7}Li breakup threshold they see a large increase in the polarization potential at the barrier energy, hence reducing the real potential at the surface. $^{9}\mathrm{Be}(\rightarrow\alpha+\alpha+n)$ has a breakup Q value of 1.57 MeV and so might be expected to behave like ^{6}Li. Observing a threshold anomaly may then come as a surprise, an indication that the cause of the thresh-

TABLE II. As Table I using a ^{9}Be density based upon shell model wave functions. The 38 MeV data set was unable to be satisfactorily fitted with this double folding calculation. R_W fixed at 1.356 fm.

E_{LAB}(MeV)	N_R	W(MeV)	a_W(fm)	NORM	χ^2_N
75	0.745	7.34	0.706	0.965	5.1
68	0.727	7.00	0.726	0.983	11.5
60	0.905	9.63	0.628	0.978	11.5
52	1.189	9.30	0.636	1.037	36.6
50	0.867	10.98	0.613	1.007	20.6
48	0.874	11.62	0.557	0.962	8.2
46	0.990	12.51	0.522	1.014	5.4
44	1.154	14.76	0.458	0.965	1.7
42	1.349	24.17	0.415	0.964	4.6
40	1.108	13.02	0.520	0.994	4.6

TABLE III. As Table I using a ^{9}Be density from an AMD model. R_W fixed at 1.354 fm.

E_{LAB}(MeV)	N_R	W(MeV)	a_W(fm)	NORM	χ^2_N
75	1.293	7.41	0.744	0.974	11.0
68	1.264	7.00	0.754	0.991	17.8
60	1.279	8.72	0.728	0.999	17.6
52	1.963	7.67	0.743	1.060	36.8
50	1.550	12.57	0.630	1.042	19.1
48	1.653	14.21	0.537	0.965	7.2
46	1.880	16.39	0.500	1.018	5.4
44	2.225	22.36	0.434	0.972	1.8
42	2.714	43.30	0.392	0.973	4.7
40	1.982	18.23	0.507	0.999	4.5
38	1.703	3.24	0.835	1.035	6.5

TABLE IV. As Table I using a ^{9}Be density from a cluster model. R_W fixed at 1.341 fm.

E_{LAB}(MeV)	N_R	W(MeV)	a_W(fm)	NORM	χ^2_N
75	0.945	7.95	0.739	0.969	5.1
68	0.921	7.63	0.757	0.989	12.2
60	1.220	11.22	0.633	0.980	11.3
52	1.533	10.21	0.671	1.044	35.3
50	1.051	13.15	0.656	1.045	19.6
48	1.150	14.40	0.561	0.963	7.9
46	1.294	16.02	0.529	1.019	5.3
44	1.530	20.67	0.459	0.968	1.7
42	1.812	37.19	0.413	0.966	4.6
40	1.410	16.67	0.531	0.997	4.6
38	1.324	3.50	0.818	1.030	6.5

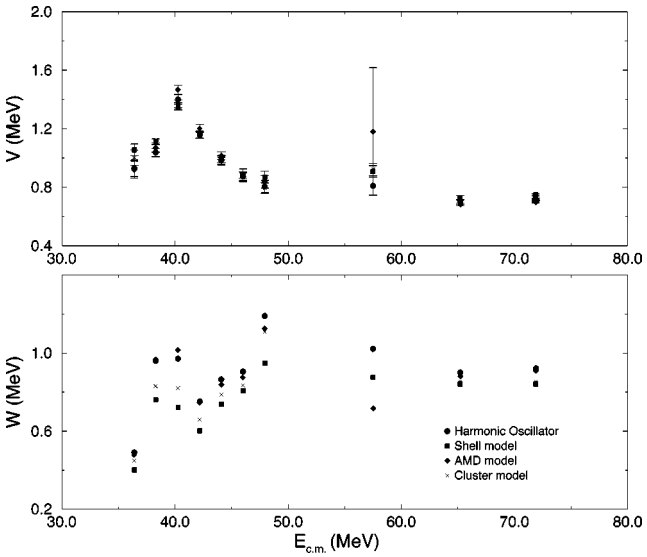

FIG. 2. Strength of the potentials at 12.3 fm. The results from all four analyses are shown. The fusion barrier is experimentally measured to be at 38.3 MeV.

old anomaly is more complicated than just the value of the dissociation threshold. It is interesting to note that all four analyses indicate a "bump" in the imaginary potential at around 40 MeV. This is reminiscent of a similar effect observed in ^{7}Li+^{208}Pb scattering [23]. Using coupled channels calculations, Keeley and Rusek [24] later ascribed this to coupling to the ^{208}Pb (^{7}Li,^{6}Li) ^{209}Pb transfer channel. It would be interesting to explore theoretically whether the bump in the present data could also be ascribed to the opening of reaction channels.

C. Dependence on the ^{9}Be density

Perhaps the most significant result from this experiment comes from the optical model analyses using different ^{9}Be radial density functions in the double folding calculation. The magnitude of the potential in the surface region and the deduced fusion cross sections (see later) are nearly identical across the analyses. This is as would be expected, as the optical model analysis is sensitive to the surface region of the potential. This is the region of interaction and so we must get the potential in this region right. Since the ^{9}Be wave functions from the different models produce different ^{9}Be densities near the surface, the double folding potentials have different surface magnitudes and so have to be renormalized by different factors N_R to get the strength of the potential in the surface region correct (as given in column 2 of Tables I–IV). The dependence of the required scaling factors N_R on the model used to determine the density of ^{9}Be results from the differences between the predictions of the models.

In the past, double folding model analyses have mainly been carried out on nuclei near closed shells. In these cases, the densities are either well known from measurement or accurate model wave functions exist. Hence it has usually been the case that the double folding potential is successful in fitting the data. The variations of N_R observed in this study reflects the ambiguity in the ^{9}Be density. While the influence of breakup upon reactions of ^{9}Be is not in dispute, this result is significant as it shows that with a "poorly" defined density (here the models disagree by 20% in the surface region), no physical conclusion may be made about the influence of coupling to the breakup channel on the elastic scattering solely based on the observation that a renormalization is needed. This should be left to coupled channel (CC) calculations. This is important for work involving diffuse nuclei near the drip line and work on exotic beams in which the structure is also less well known.

From these comments, it follows that we cannot make a critical comparison between the ^{9}Be models used in the calculations. The double folding calculation is most sensitive to the surface region density, and so this technique alone is not enough to make a critical comparison between the models, and the structural assumptions that they use. Again, CC calculations would be more suited as they would explicity include reactions which are sensitive to other radial regions.

D. Effect of the ^{9}Be quadrupole moment

One interesting issue about this system that has been raised in the literature [15,25] is the significance of the quadrupole moment on the elastic scattering cross section. The ^{9}Be nucleus is highly deformed, giving it one of the largest known quadrupole moments. It has been hypothesized [25] that it is this characteristic of the nucleus which causes any deviation of the elastic scattering cross section to that predicted by the double folding model rather than an enhanced breakup reaction channel.

The significance of the quadrupole moment in this system was tested using the quadrupole density from the ^{9}Be cluster model. A coupled channel calculation was carried out using the code FRESCO [26], in which reorientation couplings are included for the ^{9}Be ground state. The transition potential is the double folded potential between the quadrupole density and the target nucleus. No other partitions are included in the calculation, and the monopole-target potentials are those derived in this experiment. This calculation was first tested by removing the coupling to see if the code could reproduce the experimental angular distributions. This was the case, and when the coupling was included, the changes to the angular distribution were too small to have any effect on the potential parameters extracted from the optical model fit.

IV. FUSION CROSS SECTION CALCULATIONS

The fusion cross section for a system may be estimated from the optical potential using a one-dimensional barrier penetration approach. In this method, the energy dependent real potential extracted from the optical model fitting procedure is used to generate the total potential (nuclear + Coulomb + centrifugal) for each partial wave. The fusion cross section is the sum of the partial wave transmission coefficients [27]:

$$\sigma_F(E) = \frac{\pi}{k^2}\sum_{l=0}^{\infty}(2l+1)T_l(E). \qquad (2)$$

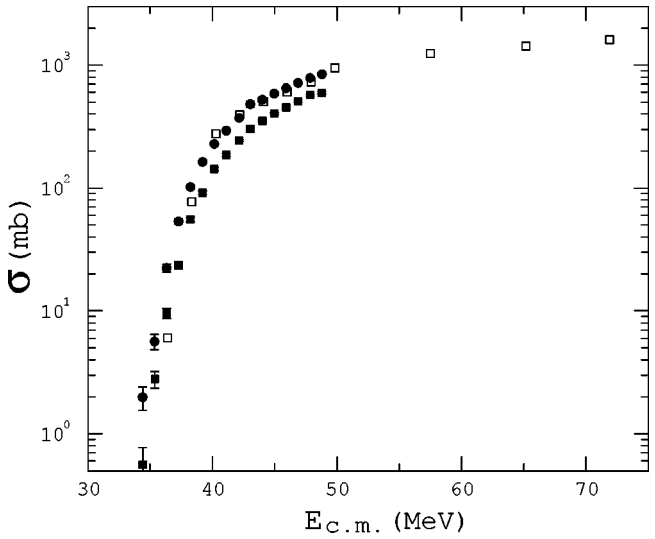

FIG. 3. Calculated fusion cross sections deduced from the optical model potentials using the shell model density (open squares). The filled data points are measured cross sections for complete fusion (squares) and complete + partial fusion (circles) [14].

The calculation of the transmission coefficients t_l was performed using the WKB subroutine in FRESCO [26]. The calculation was repeated using the optical potentials obtained using all four ^{9}Be density functions. The results are very close and are plotted in Fig. 3, for the shell model density, along with recent experimental data of the complete and partial fusion cross sections [16]. Our results are in agreement with the sum of the complete and partial fusion cross sections. Dasgupta *et al.* [16] observed that in this system there was a significant amount of partial fusion, but showed that a CC calculation predicted the amount of fusion to be approximately equal to the sum of partial and complete fusion. The prediction of the fusion using the optical potential is in agreement with both the previous CC calculation and the measured sum of the complete and partial fusion cross sections. We interpret this to imply that although breakup may remove flux from the entrance (elastic) channel, which would otherwise have led to fusion, the two seem to be balanced. We cannot, however, say that if the projectile approaches on a trajectory which in the absence of breakup would lead to fusion, and that it is still committed to this even if breakup occurs, the only difference being that it appears in the partial fusion channel. While such questions can be addressed theoretically in the context of coupled reaction channel calculations, at present no experimental method is available to distinguish such subtleties in the reaction.

V. SUMMARY

The elastic scattering cross sections for the ^{9}Be+^{208}Pb system have been measured at 11 energies ranging from 38 to 75 MeV. The results have been fitted within an optical model framework employing a microscopic real potential and a phenomenological imaginary part. The surface strength of the real part increased significantly as the Coulomb barrier energy was approached; a threshold anomaly. The deformation of the ^{9}Be nucleus has been shown not to influence the elastic scattering analysis to any significant degree.

Comparison of fusion cross sections deduced from the elastic potential and experimentally observed cross sections demonstrates that breakup inhibits the complete fusion channel. There appears to be a rough balance between the flux removed from complete fusion and that fed into incomplete fusion.

Finally, it has been shown that the renormalization factor N_R required to achieve an optimum fit to experimental elastic scattering cross section cannot by itself be used to infer the effect of breakup, as it has been practiced in the past. The value depends on the accuracy of the density used in the evaluation of the double folded potential. In situations where the nuclear density function is not precisely known no physical conclusions may be made from the renormalization factor alone. It remains to be seen whether the approach is sensitive enough for this process to be used as a test of the validity of wave functions for these weakly bound systems.

ACKNOWLEDGMENTS

R.J.W. would like to thank the EPSRC for financial assistance during the period this work was carried out. We would also like to thank Dr. N. M. Clarke for providing copies of HIOPTIM and DFPOT and Professor I. J. Thompson for calculating the point nucleon density from [21]. We would also like to thank the authors of Refs. [22,9,10] for providing us with tabulated versions of their density functions.

[1] G. Satchler and W. Love, Phys. Rep. **55**, 183 (1979).
[2] N. Keeley, S. Bennett, N. Clarke, G. Tungate, P. Drumm, M. Nagarajan, and J. Lilley, Nucl. Phys. **A571**, 326 (1994).
[3] G. Keeley, N. Davis, R. Ward, B. Fulton, G. Tungate, N. Kelley, K. Rusek, E. Bartosz, P. Cathers, D. Caussyn, T. Drummer, and K. Kemper, Phys. Rev. C **63**, 024601 (2000).
[4] C. Signorini, Z. Liu, A. Yoshida, T. Fukuda, Z. Liu, K. Löbner, L. Müller, Y. Pu, K. Rudolph, F. Soramel, C. Zotti, and J. Sida, Eur. Phys. J. A **2**, 227 (1998).
[5] G. Bertsch *et al.*, Nucl. Phys. **A284**, 399 (1977).
[6] Y. Eisen *et al.*, Phys. Lett. **63B**, 253 (1976).
[7] Y. Sakuragi, M. Yahiro, and M. Kamimura, Prog. Theor. Phys. **70**, 1047 (1983).
[8] Y. Sakuragi, M. Yahiro, and M. Kamimura, Prog. Theor. Phys. **89**, 136 (1986).
[9] K. Arai, Y. Ogawa, Y. Suzuki, and K. Varga, Phys. Rev. C **54**, 132 (1996).
[10] Y. Kanada-En'yo, H. Horiuchi, and A. Ono, Phys. Rev. C **52**, 628 (1995).
[11] J. Lilley, B. Fulton, M. Nagarajan, and I. Thompson, Phys. Lett. **151B**, 181 (1985).
[12] B. Fulton, in *Heavy Ion Collisions at Energies Near the Cou-*

lomb Barrier, edited by M. Nagarajan, Inst. Phys. Conf. Ser. 110 (IOP, Bristol, 1990).
[13] G. Satchler, Phys. Rep. **199**, 147 (1991).
[14] N. Keeley and K. Rusek, Phys. Lett. B **427**, 1 (1998).
[15] C. Signorini *et al.*, Phys. Rev. C **61**, 061603(R) (2001).
[16] M. Dasgupta *et al.*, Phys. Rev. Lett. **82**, 1395 (1999).
[17] C. Signorini *et al.*, Eur. Phys. J. A **5**, 7 (1999).
[18] R. J. Woolliscroft, N. M. Clarke, B. R. Fulton, R. L. Cowin, M. Dasgupta, D. J. Hinde, C. R. Morton, and A. C. Berriman, Phys. Rev. C **68**, 014611 (2003).
[19] N. Clarke (unpublished).
[20] M. Brandan and G. Satchler, Phys. Rep. **285**, 143 (1997).
[21] V. Hnizdo, J. Szymakowski, K. Kemper, and J. Fox, Phys. Rev. C **24**, 1495 (1981).
[22] G. Satchler, Phys. Lett. **83B**, 284 (1979).
[23] I. Martel *et al.*, Nucl. Phys. **A582**, 357 (1995).
[24] N. Keeley and K. Rusek, Phys. Rev. C **56**, 3421 (1997).
[25] V. Hnizdo, K. Kemper, and J. Szymakowski, Phys. Rev. Lett. **46**, 590 (1981).
[26] I. Thompson, Comput. Phys. Rep. **2**, 167 (1988).
[27] P. Fröbrich and R. Lipperheide, *Theory of Nuclear Reactions* (Clarendon Press, Oxford, 1996).
[28] For a full listing of the experimental results, see EPAPS Document No. E-PRVCAN-69-055404. A direct link to this document may be found in the online article's HTML reference section. The document may also be reached via the EPAPS homepage (http://www.aip.org/pubservs/epaps.html) or from ftp.aip.org in the directory /epaps/. See the EPAPS homepage for more information.